Acoustic properties of air-saturated porous materials containing dead-end porosity

Thomas Dupont, Philippe Leclaire, Olivier Sicot, Xiao-Lu Gong, Raymond Panneton

Acoustic properties of air-saturated porous materials containing dead-end porosity

T. Dupont[1], P. Leclaire[2], O. Sicot,
LRMA - DRIVE, Université de Bourgogne, 49 rue Mademoiselle Bourgeois, 58027 Nevers cedex,

X. L. Gong,
LASMIS, Université de Technologie de Troyes (UTT), FRE CNRS 2848, 12 rue Marie Curie -BP 2060- 10010 Troyes Cedex

R. Panneton[3]
GAUS, Department of Mechanical Engineering, Univ. de Sherbrooke, Sherbrooke, Que., Canada J1K 2R1

This study examines the acoustic properties of materials with complex micro-geometry containing partially open or dead-end porosity. One of these kinds of materials can be obtained from dissolving salt grains embedded in a solid metal matrix with the help of water. The solid matrix is obtained after the metal in liquid form has invaded the granular material formed by the salt particles at negative pressure and high temperature, and after cooling and solidification of the metal. Comparisons between theoretical and experimental results show that the classical Johnson-Champoux-Allard model does not quite accurately predict the acoustic behavior. These results suggest that the assumptions of the Biot theory may not be all fulfilled and that Helmholtz-type resonators and dead ends can be present in the material. The first part of the study proposes a simple model to account for this geometry. Based on this model, two acoustic transfer matrices are developed: one for non symmetric and one for symmetric dead-end porous elements. This model can be used to study the acoustic absorption and sound transmission properties of the type of material described above. In the second part, a series of simplified samples are proposed and tested with a three-microphone impedance tube to validate the exposed model. Finally, the third part compares predictions of the exposed model to impedance tube results on a real aluminum foam sample containing dead-end pores.

[1] thomas.dupont@u-bourgogne.fr
[2] philippe.leclaire@u-bourgogne.fr
[3]Raymond.Panneton@usherbrooke.ca

I. INTRODUCTION

Air-saturated porous metals such as porous aluminum may be used in numerous applications such as thermal exchangers or shock absorbers in the automobile and aircraft industries. These materials also exhibit interesting acoustic properties. In many applications, they can withstand fairly high temperatures, they can be used in hostile environments (fluid projection, flames) and they are durable and stable in time.

The metal foam obtained following the fabrication process[1] depicted in Figure 1 is behind the motivation of the exposed work. In this process, melted aluminum is poured in a container filled with salt grains. The melting temperature of aluminum is 660°C while that of the sodium chloride (NaCl) is 801°C. Melted aluminum can therefore fill the interstitial spaces between the solid grains. A negative pressure suction is applied in order to facilitate the flow. The grain size distribution can be controlled by successive sieving of the salt grains. After the metal has cooled down, the sample is cut and plunged in water to dissolve the sodium chloride. Then the sample is dried, air replaces the space formerly occupied by the solid grains and the sample porous metal is created. Figure 2 shows an aluminum foam resulting from this fabrication process.

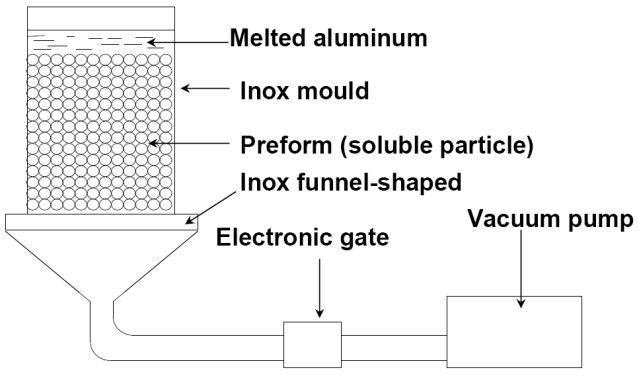

Figure 1: Principle of the making of aluminum foams[1].

At first sight, the observation of the microstructure and characteristic size of the pores suggest that an equivalent fluid model is well adapted to study the acoustic properties of the resulting foam. In the past, equivalent fluid models have been derived to describe the acoustic

wave propagation in rigid-frame open-cell porous media saturated by air.[2] The model used in the exposed work is that of Johnson-Champoux-Allard. This phenomenological model is accurate and has been applied successfully to sound absorbing materials such as polyurethane foams or fibrous materials[2-4].

In this article, it is experimentally shown that a classical equivalent fluid model is not as accurate as expected for the studied metallic foams: it appears that not all the assumptions of the classical model are fulfilled. In particular, a closer look at the microstructure (Figure 2) seems to show that some pores are connected to the exterior by one end only. Observation using three-dimensional pictures obtained by a micro-tomography approach confirms the presence of dead-end porosity in these metallic foams.

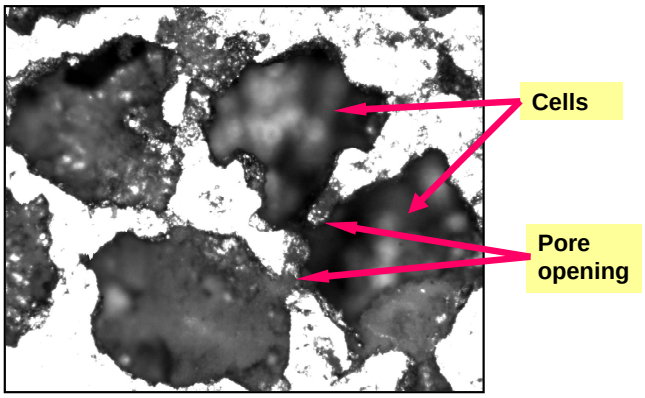

Figure 2: Microstructure of the porous metallic foam[1].

As summarized in Figure 3, the hydrogeology scientist distinguishes different kinds of porosities:[5,6]

- Total porosity is defined as the ratio between the air volume (volume without material) and the total volume of the sample in a homogeneous area (representative sample). This porosity includes closed and open porosities.

- Closed porosity (also called residual porosity) represents the cells that are completely closed (not interconnected with others cells). In the rigid frame approach these cells do not influence the acoustical behavior of material.

- Open porosity (also called effective porosity or connected porosity) is defined as the ratio of interconnected pores to the bulk volume of the porous material. This is the ratio between the “mobile volume” of saturation water released under the effect of a complete drainage and the total volume of the sample. This porosity includes kinematic and dead end porosities.

- Kinematic porosity, is related to the displacement of water moving in a permeable medium. It is equivalent to the ratio of the volume of the interstices truly traversed by moving water and the total volume of the medium. The kinematic porosity is the one used in the Biot model and is therefore referred to as the "Biot porosity" in the remaining of this paper.

- Dead-end porosity (that can also be referred to as "ink bottle porosity") is defined as the ratio of the volume of non moving water in closed cells to the bulk volume of the porous material; it represents the cells that, although connected to another cell and to the exterior at one end, remain closed at the other end. Bear,[7] who in 1979 worked on interconnected pore space, stated that the porous medium contains dead-end pores, corresponds to material which partially contains pores or channels with only a narrow single connection to the interconnected pore space, so that almost no flow occurs through them.

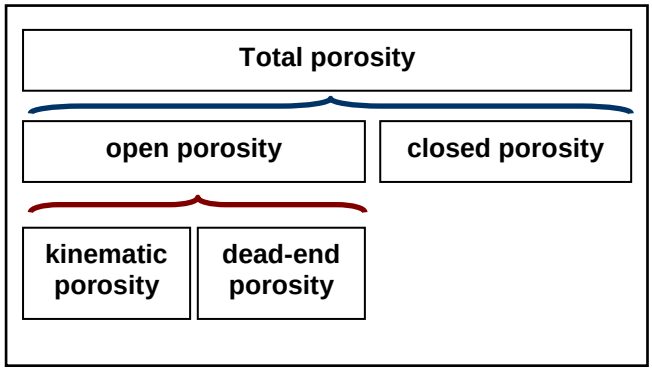

Figure 3: Illustration showing different porosity levels.

Gibb[8] presented a study which documents the laboratory technique for measuring effective porosity of fine-grained soils. This approach is based on the travel time measurement though the media. Migration or flow through a porous media can be evaluated by means of tracers. These techniques are difficult to use and are not well adapted to all porous media. Zwikker and Kosten[6] noticed the effect of dead-end porosity on the acoustic properties of material, but

they did not offer a theoretical description of this phenomenon. Previous studies[9-11] noticed that the presence of dead-end pores seems to modify the permeability, tortuosity and flow resistivity. More recently, Chevillote *et al.*[12] studied the sound-absorption predictions of perforated closed-cell metallic foams. They chose a microstructure-based model approach, and they compared the model with the experimental results. The porous media used in their study included dead-end pores created by perforating solids incorporating gas inclusions (closed porosity). They observed that the dead-end pores could have significant effects on the media acoustic behavior.

To model the acoustic behavior of this kind of porous material, it is therefore important to take into account the effect of dead-end pores. This complex geometry is not taken into account in the classical equivalent fluid models[2]. Based on a simple approach, a new model is proposed to account for the presence of dead-end porosity in the material as well as the complexity of pore shapes. It includes two new parameters in addition to the five parameters (Biot porosity, tortuosity, static flow resistivity, viscous and thermal characteristic lengths) of the classical Johnson-Champoux-Allard model. The new parameters are: the dead-end porosity ϕ_{DE} and an average length of the dead-end pores l_{DE}. Comparison of the results provided by the modified model with experimental results seems to give a better match. In order to validate the present model, a comparison between theoretical and experimental results was carried out on a "simplified sample" (sample with well-controlled microstructural parameters) and on a porous metallic foam that is likely to incorporate dead end pores. Sections of the present article were presented at a conference.[13]

II. MODEL FOR DEAD-END POROSITY

A. Simple model at the microscopic scale

As mentioned above, dead-end porosity is known in geophysics[4] and its effects has been observed on some porous materials in acoustics.[4,9-12,14] However, to our knowledge no refined model of acoustic wave propagation in media with this micro-structural feature has been published.

Figure 2 also reveals the presence of narrow channels between the cavities. These very narrow constrictions are thought to be the cause of rotational flow with nonzero vorticity; however, this phenomenon is not studied here.

The presence of dead-end porosity in the studied materials is initially modeled at the microscopic level in terms of acoustic admittances, and then a homogenized version of a microscopic relationship between admittances is proposed. First of all, a circular duct of constant cross section S is considered as shown in Figure 4. This duct is acoustically characterized by its characteristic impedance Z. The right end of the duct is connected to two auxiliary ducts 1 and 2 of respective characteristic impedances Z_1 and Z_2, in the configuration of a Y-shape junction. The two branches after the crossroad are also of constant section S_1 and S_2, respectively.

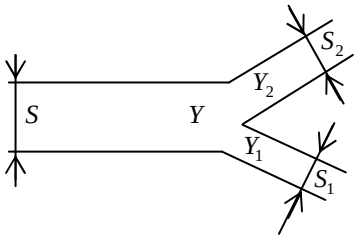

Figure 4: Y-shape junction between three branches in a porous medium.

This problem is a classical academic problem[15] and, assuming a left-to-right propagation from the principal branch to the secondary branches, the following relationship exists between admittances:

$$Y = Y_1 + Y_2 , \qquad (1)$$

where Y, Y_1 and Y_2 are respectively the acoustic admittances of the main branch and of branches 1 and 2, related to the characteristic impedance of each branch through the following relations:

$$Y = \frac{S}{Z}, \quad Y_1 = \frac{S_1}{Z_1}, \quad Y_2 = \frac{S_2}{Z_2}. \qquad (2)$$

The characteristic impedances Z, Z_1 and Z_2 normalized by the sections are referred to as "acoustic impedances."[15]

It is now considered that one of the branches – branch 1 for example – is closed (see Figure 5). The previous relation (1) remains valid with the difference that Y now represents a local admittance at the end of the main branch while Y_1 corresponds to the local admittance at the entrance of branch 1.

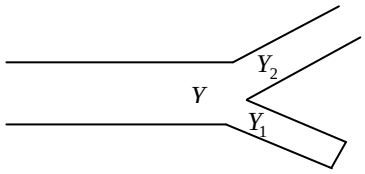

Figure 5: Y-shape junction in a porous medium with one branch closed.

If branch 1 has a constant cross section and if the closing wall is rigid and perpendicular to the branch axis, the admittance Y_1 is given by:

$$Y_1 = \frac{S_1}{-j\,Z_C\,cotan(kl)}, \qquad (3)$$

where Z_C is the characteristic impedance of air, k the wavenumber, l the length of branch 1 and j the unit imaginary complex number (a time dependence in $exp(j\omega t)$ has been chosen, ω being the angular frequency).

B. Model at the macroscopic scale and average length of the dead ends

It is assumed that, at the considered frequencies, the wavelengths are much greater than the characteristic sizes of the microstructure. The behavior described at the microscopic scale can then be homogenized:

$$\overline{Y} = \overline{Y_1} + \overline{Y_2}, \qquad (4)$$

where $\overline{Y}$, $\overline{Y_1}$ et $\overline{Y_2}$ represent the averaged quantities associated with Y, Y_1 et Y_2, respectively, in a homogenization volume in the porous medium. In addition, it is assumed that in the

studied materials, the cross sections of all branches are statistically uniform so that they do not play a role in equation (4).

This last equation can be easily interpreted. For a linear propagation, the acoustic behavior of a material containing dead-end pores is given by the sum of two contributions: $\bar{Y}_2$ associated with the fully open pores and $\bar{Y}_1$ associated with the partially open pores (dead-end pores). The volume proportion of the dead-end pores will be noted ϕ_{DE} (for $\phi_{Dead\ End}$) while the porosity of the fully opened pores will be noted ϕ_B (for ϕ_{Biot}). These two porosities are related to the total open porosity through the relation:

$$\phi = \phi_B + \phi_{DE} . \qquad (5)$$

A pore can be considered "fully opened" if, when considering a slab of material at the laboratory scale, one can find a path connecting the front and the rear surface of the slab, the pore being connected to the exterior by both ends. A "partially opened" or "dead-end" pore would be one with only one end connected to either the front or the rear surface of the slab. It is important to make a distinction between the "opened porosity" ϕ and the porosity of the "connected effective pores" ϕ_B (the former will always be greater than or equal to the latter). Among the open pores, some can be closed at one end.

The $\bar{Y}_2$ contribution is that of the pore that verifies the assumptions of the Johnson-Champoux-Allard model. It can be expressed as:

$$\bar{Y}_2 = \frac{1}{\bar{Z}_B} , \qquad (6)$$

where $\bar{Z}_B$ is the characteristic impedance of the classical model, defined only for fully opened pores of porosity ϕ_B.

From (3), one can define for $\bar{Y}_1$ an average value, integrated over a homogenization volume V_{DE} of dead end pores:

$$\bar{Y}_1 = \frac{j}{Z_C} \frac{\iiint_{V_{DE}} \tan(kl) dV}{\iiint_{V_{DE}} dV}. \qquad (7)$$

If the additional assumption $kl << 1$ is made, equation (7) becomes, to the first order:

$$\bar{Y}_1 \approx \frac{jk}{Z_C} \frac{\iiint_{V_{DE}} l dV}{\iiint_{V_{DE}} dV}. \qquad (8)$$

This assumption is valid for dead-end pores that are much shorter than any acoustic wavelength. This allows us to define an average length of the dead-end pores by:

$$l_{DE} = \frac{\iiint_{V_{DE}} l dV}{\iiint_{V_{DE}} dV}. \qquad (9)$$

The admittance (8) is finally expressed as:

$$\bar{Y}_1 \approx \frac{jkl_{DE}}{Z_C}. \qquad (10)$$

To illustrate this approach, an example of a material with simple geometries is proposed (see Figure 6 in this material, it is clear that $l_{DE} = d$. With definition (9), this result is easily retrieved:

$$l_{DE} = \frac{\iiint_{V_{DE}} l dV}{\iiint_{V_{DE}} dV} = \frac{Vd + Vd + ... + Vd}{V + V + ... + V} = \frac{nVd}{nV} = d. \qquad (11)$$

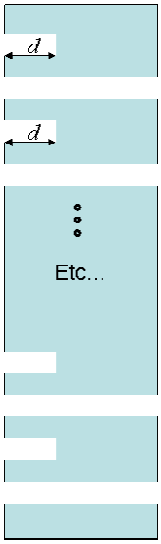

Figure 6: Example of a material with simple geometries, used to illustrate the l_{DE} formulation.

Remark:

In the framework of the effective fluid approach of Biot[16,17], the following length could be defined (instead of that of equation 9):

$$l_{DE}^{eff} = \frac{\iiint_V l \, dV}{\iiint_V dV}, \qquad (12)$$

where V is a homogenization volume of bulk material involving the porous aggregate (solid + fluid).

C. Accounting for dissipations in dead-end pores

The previous equations for $\overline{Y}_1$ were established from a simple modeling of a dead-end pore at the microscopic scale as a closed duct. To account for viscous and thermal dissipations in the dead-end pores at the macroscopic scale, it suffices to replace Z_C and k by those provided by the Johnson-Champoux-Allard model applied to the volume fraction of dead-end pores

$$Z_C \to \overline{Z}_{DE} \quad \text{and} \quad k \to \overline{k}_{DE}\,. \qquad (13a)$$

while when applied to the volume fraction of the kinematic pores (the Biot porosity), one should use

$$Z_C \to \overline{Z}_B \quad \text{and} \quad k \to \overline{k}_B\,. \qquad (13b)$$

Other remarks can be made about the model:

a) Equation (4) indicates that the sole contribution $\overline{Y_2}$ would correspond to a simple porosity correction. The additional contribution $\overline{Y_1}$ accounts for the standing wave fields created in the dead-end pores.

b) The principle of the model of acoustic wave propagation in porous materials including dead-end pores can be summarized with the schematic shown in Figure 7.

c) The assumptions of the proposed model are the same as those of the classical model. One additional assumption has been added on the length of the dead-end pores.

d) This model does not account for the presence of narrow constrictions in the material that are thought to be responsible for local flows with vorticity, even at low average flow velocity.

D. Recall of the Johnson-Champoux-Allard model

This section recalls the main results of the Johnson-Champoux-Allard model.[2,4,18] This model is based on five macroscopic parameters: porosity ϕ, static airflow resistivity σ, tortuosity α_∞, viscous characteristic length Λ, and thermal characteristic length Λ'. In the rigid-frame approximation, the solid matrix (skeleton) is considered much heavier and more rigid than the saturating air. As pointed out by Panneton,[19] several approaches (effective or equivalent approaches) can be used to describe the complex density and bulk modulus of the slab. The approach used here consists in considering the slab of porous material in the rigid frame approximation as a slab of equivalent fluid with the following density $\rho_{eq}(\omega)$ and bulk modulus $K_{eq}(\omega)$:

$$\rho_{eq}(\omega) = \frac{\alpha_\infty \rho_f}{\phi}\left(1 - j\frac{\omega_c}{\omega}F(\omega)\right), \qquad (14)$$

$$K_{eq}(\omega) = \frac{1}{\phi}\frac{\gamma P_0}{\gamma - (\gamma-1)\left(1 - j\frac{8\eta}{B^2\omega\Lambda'^2\rho_f}G(B^2\omega)\right)^{-1}}, \qquad (15)$$

with

$$\omega_c = \frac{\sigma\phi}{\rho_f \alpha_\infty}, \qquad (16)$$

where η is the dynamic viscosity, B^2 the Prandtl number, γ the constant pressure and volume specific heat ratio (sometimes referred to as the adiabatic constant), and P_0 the atmospheric static pressure. The parameter ω_c is Biot's cut off angular frequency separating Biot's high and low frequency ranges.

The functions $F(\omega)$ and $G(B^2\omega)$ are the correction functions introduced respectively by Johnson et al[18] and by Champoux and Allard.[4] They are given by:

$$F(\omega) = \sqrt{1 + j\frac{4\eta\rho_f \alpha_\infty^2}{\phi^2 \sigma^2 \Lambda^2}\omega}, \qquad (17)$$

and

$$G(B^2\omega) = \sqrt{1 + j\frac{\rho_f \Lambda'^2 B^2 \omega}{16\eta}}. \qquad (18)$$

All the necessary parameters for the acoustic characterization of porous layers are easily deduced with the help of $\rho_{eq}(\omega)$ and of $K_{eq}(\omega)$. In particular, the characteristic impedance and wave number of are given by:

$$\bar{Z}(\omega) = \sqrt{\rho_{eq}(\omega) K_{eq}(\omega)} \quad \text{and} \quad \bar{k}(\omega) = \omega\sqrt{\frac{\rho_{eq}(\omega)}{K_{eq}(\omega)}}. \qquad (19)$$

It is worth mentioning that these expressions (ρ_{eq}, K_{eq}, $\bar{Z}$, $\bar{k}$) can be applied to the open pores and to the dead-end pores with special attention on the choice of the macroscopic properties (notably $\phi = \phi_{DE}$ for the dead-end domain, and $\phi = \phi_B$ for the Biot domain).

E. Correction of the Johnson-Champoux-Allard model to include dead-end pores

The correction that includes the effect of dead-end pores is implemented through the use of equations (4), (5), (6) and (10) in order to calculate $\bar{Y}(\phi)$. Following Figure 7, the Johnson-Champoux-Allard model is first applied on a material of porosity ϕ_B to determine $\bar{Y}_2(\phi_B)$ and

then a second time in order to determine $\overline{Y}_1(\phi_{DE})$. In the second application of the model, a slab of thickness l_{DE} and of porosity ϕ_{DE} must be considered. The acoustical properties of the material containing dead-end pores are finally deduced from $\overline{Y}(\phi)$ given by equation (4).

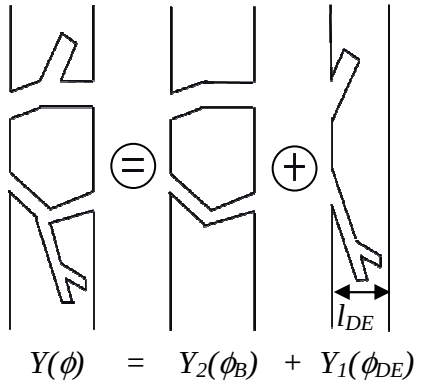

Figure 7: Principle of the model including dead-end pores.

F. Transfer matrix method

In acoustics, the transfer matrix method is a powerful method to optimize and predict sound absorption and sound transmission of single layer and multilayer sound absorbing materials[2]. In what follows, transfer matrices will be developed for the studied rigid-frame porous aggregate containing dead-end porosity for non-symmetric and symmetric configurations.

F-1 Non-symmetric configuration

A vertically periodic unit cell of a non-symmetric porous medium with dead-end porosity is shown in Figure 8. Here the porous medium separates two fluid domains. The cell is divided into two porous elements in parallel. The first element (element DE) is the one representing the dead-end porosity (non symmetric element). The second one is the BIOT element containing pores that are opened on both ends only (symmetric element), the whole being non-symmetric. Each element has equivalent macroscopic properties averaged over a representative homogeneous volume. To link acoustic pressures and velocities on both faces of the material, a transfer matrix relation can be developed.

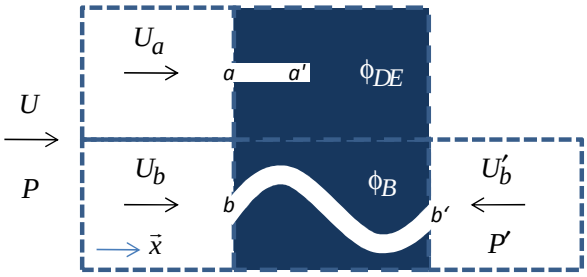

Figure 8: Principle of the model including non symmetric dead-end element

For the DE element, the transfer matrix relation is given by:

$$\begin{Bmatrix} P_a \\ U_a \end{Bmatrix} = [T]^{DE} \begin{Bmatrix} P'_a \\ -U'_a \end{Bmatrix}, \qquad (20)$$

with

$$[T]^{DE} = \begin{bmatrix} t_{11}^{de} & t_{12}^{de} \\ t_{21}^{de} & t_{22}^{de} \end{bmatrix} = \begin{bmatrix} \cos(\bar{k}_{DE} l_{DE}) & j\bar{Z}_{DE} \sin(\bar{k}_{DE} l_{DE}) \\ \frac{j}{\bar{Z}_{DE}} \sin(\bar{k}_{DE} l_{DE}) & \cos(\bar{k}_{DE} l_{DE}) \end{bmatrix}, \qquad (21)$$

where the prime symbol is assigned to an output port variable, and the averaged length and equivalent fluid properties are obtained from Eqs. (9) and (19), respectively. Here, the minus sign is added to take into account that velocity is defined following the inward normal to the element. Since the elements are in parallel, it is preferred to work with admittances as presented in Sec. II.A. Consequently, Eq. (20) can be rewritten in terms of an admittance matrix as

$$\begin{Bmatrix} U_a \\ U'_a \end{Bmatrix} = [Y]^{DE} \begin{Bmatrix} P_a \\ P'_a \end{Bmatrix}, \qquad (22)$$

with

$$[Y]^{DE} = \begin{bmatrix} y_{11}^{de} & y_{12}^{de} \\ y_{21}^{de} & y_{22}^{de} \end{bmatrix} = \begin{bmatrix} \frac{t_{22}^{de}}{t_{12}^{de}} & -\frac{1}{t_{12}^{de}} \\ -\frac{1}{t_{12}^{de}} & \frac{t_{11}^{de}}{t_{12}^{de}} \end{bmatrix}. \qquad (23)$$

Since at the end of the dead-end pore the velocity vanishes ($U'_a = 0$), the previous transfer matrix yields

$$P_a' = -\frac{y_{21}^{de}}{y_{22}^{de}} P_a . \qquad (24)$$

For the BIOT element, the transfer matrix relation is given by

$$\begin{Bmatrix} P_b \\ U_b \end{Bmatrix} = [T]^B \begin{Bmatrix} P_b' \\ -U_b' \end{Bmatrix}, \qquad (25)$$

with

$$[T]^B = \begin{bmatrix} t_{11}^b & t_{12}^b \\ t_{21}^b & t_{22}^b \end{bmatrix} = \begin{bmatrix} \cos(\bar{k}_B l) & j\bar{Z}_B \sin(\bar{k}_B l) \\ \frac{j}{\bar{Z}_B}\sin(\bar{k}_B l) & \cos(\bar{k}_B l) \end{bmatrix}, \qquad (26)$$

where the equivalent fluid properties are respectively obtained from Eqs. (9) and (19) and correspond to the porous material without dead-end pores. The corresponding admittance matrix is given by

$$\begin{Bmatrix} U_b \\ U_b' \end{Bmatrix} = [Y]^B \begin{Bmatrix} P_b \\ P_b' \end{Bmatrix}, \qquad (27)$$

with

$$[Y]^B = \begin{bmatrix} y_{11}^b & y_{12}^b \\ y_{21}^b & y_{22}^b \end{bmatrix} = \begin{bmatrix} \frac{t_{22}^b}{t_{12}^b} & -\frac{1}{t_{12}^b} \\ -\frac{1}{t_{12}^b} & \frac{t_{11}^b}{t_{12}^b} \end{bmatrix}. \qquad (28)$$

Invoking continuity of pressure ($P = P_a = P_b$) and continuity of flow rate ($SU = S(U_a + U_b)$) at the air-element interfaces, Eqs.(22), (24) and (28) yield

$$\begin{cases} U = \left(y_{11}^b + y_{11}^{de} - \frac{\left(y_{12}^{de}\right)^2}{y_{22}^{de}} \right) P + y_{12}^b P_b' \\ U_b' = y_{12}^b P + y_{22}^b P_b' \end{cases}. \qquad (29)$$

Here, it is worth mentioning that U_a and U_b are the macroscopic fluid velocity in the fluid domain in front of each element, respectively. They are related to the velocity in the pores by $U_a = \phi_{DE} u_a$ and $U_b = \phi_B u_b$. Consequently, this yields, at the macroscopic scale, the continuity of velocity: $U = \phi_{DE} u_a + \phi_B u_b$.

Solving Eq. (29) for *P* and *U*, the non symmetric matrix system can be written as

$$\begin{Bmatrix} P \\ U \end{Bmatrix} = [T]^{NS} \begin{Bmatrix} P_b' \\ -U_b' \end{Bmatrix}, \qquad (30)$$

with

$$[T]^{NS} = \frac{1}{y_{12}^b} \begin{bmatrix} -y_{22}^b & -1 \\ \left(y_{12}^b\right)^2 - y_{22}^b \left(y_{11}^b + y_{11}^{de} - \dfrac{\left(y_{12}^{de}\right)^2}{y_{22}^{de}} \right) & -\left(y_{11}^b + y_{11}^{de} - \dfrac{\left(y_{12}^{de}\right)^2}{y_{22}^{de}} \right) \end{bmatrix}. \qquad (31)$$

Matrix $[T]^{NS}$ is the transfer matrix of the two elements in parallel. Index *NS* is chosen for *Non Symmetric* dead-end element. This system preserves the reciprocity principle since $\det[T]^{NS} = 1$; however it is not of symmetric nature (i.e. $t_{11}^{ns} \neq t_{22}^{ns}$). The validation of this approach will be discussed in the experimental part of the present study.

F-2 Symmetric configuration

Now, the element is assumed symmetric, it means that dead-end pores are seen on both faces of the equivalent element. This type of element is shown in Figure 9. For this case, the previous approach is used to establish the transfer matrix of the porous aggregate with dead-end porosity.

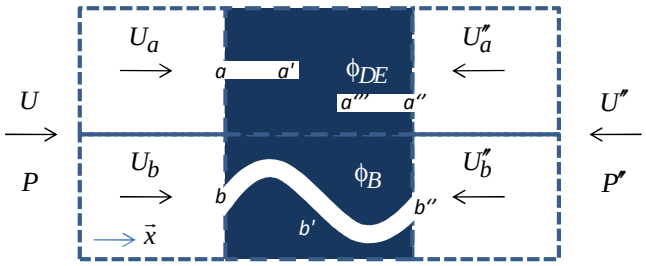

Figure 9: Principle of the model including symmetric dead-end element

At first, it is important that the BIOT element be divided in two along the thickness. Consequently, the sample has a thickness half the total thickness (i.e. $l \rightarrow l/2$) and the middle is located at point *b'*. It is assumed that the DE and BIOT elements have homogeneous properties along the thickness. In this case, porosities ϕ_{DE} and ϕ_B are the same for the first and second halves. Note that since the dead-end porosity is seen equivalently by incident waves on both faces of the sample, the dead-end pore thickness is the same for the first and second

halves and is given by the averaged length l_{DE}. Even if in Figure 9 dead-end porosity seems virtually doubled, the porosity stays ϕ_{DE}.

With the previous description, the transfer matrix of the first half is computed as done in the previous section. The only change is to use *l/2* instead of *l*. In this case, the transfer matrix relation of the first half is written as

$$\begin{Bmatrix} P \\ U \end{Bmatrix} = [T]_A \begin{Bmatrix} P'_b \\ -U'_b \end{Bmatrix}, \qquad (32)$$

where $[T]_A = [T(l/2)]^{NS}$ is the transfer matrix of the first half of the porous aggregate with dead-end porosity on the front surface.

For the second half, a similar development is done. For the dead-end pore on the right, the following relations are developed

$$\begin{Bmatrix} P'''_a \\ U'''_a \end{Bmatrix} = \begin{bmatrix} t^{de}_{11} & t^{de}_{12} \\ t^{de}_{21} & t^{de}_{22} \end{bmatrix} \begin{Bmatrix} P''_a \\ -U''_a \end{Bmatrix}, \qquad (33)$$

and

$$\begin{Bmatrix} U''_a \\ U'''_a \end{Bmatrix} = \begin{bmatrix} y^{de}_{11} & y^{de}_{12} \\ y^{de}_{21} & y^{de}_{22} \end{bmatrix} \begin{Bmatrix} P''_a \\ P'''_a \end{Bmatrix}. \qquad (34)$$

With the boundary condition $U'''_a = 0$, the previous equation yields

$$P'''_a = -\frac{y^{de}_{21}}{y^{de}_{22}} P''_a. \qquad (35)$$

For the second half of the BIOT element (i.e., from *b'* to *b''*), the following relations are developed

$$\begin{Bmatrix} P'_b \\ U'_b \end{Bmatrix} = \begin{bmatrix} t^{b}_{11} & t^{b}_{12} \\ t^{b}_{21} & t^{b}_{22} \end{bmatrix} \begin{Bmatrix} P''_b \\ -U''_b \end{Bmatrix}, \qquad (36)$$

and

$$\begin{Bmatrix} U'_b \\ U''_b \end{Bmatrix} = \begin{bmatrix} y^{b}_{11} & y^{b}_{12} \\ y^{b}_{21} & y^{b}_{22} \end{bmatrix} \begin{Bmatrix} P'_b \\ P''_b \end{Bmatrix}. \qquad (37)$$

Invoking continuity of pressure and continuity of flow rate at the air-element interfaces, and solving for P_b' and U_b', the transfer matrix relation of the second half is written as

$$\begin{Bmatrix} P_b' \\ U_b' \end{Bmatrix} = [T]_B \begin{Bmatrix} P'' \\ -U'' \end{Bmatrix}, \qquad (38)$$

where $[T]_B$ is the transfer matrix of the second half of the porous aggregate with dead-end porosity on the rear surface. It is given by

$$[T]_B = \frac{1}{y_{12}^b} \begin{bmatrix} -\left(y_{22}^b + y_{22}^{de} - \frac{\left(y_{12}^{de}\right)^2}{y_{11}^{de}} \right) & -1 \\ \left(y_{12}^b\right)^2 - y_{11}^b \left(y_{22}^b + y_{22}^{de} - \frac{\left(y_{12}^{de}\right)^2}{y_{11}^{de}} \right) & -y_{11}^b \end{bmatrix}. \qquad (39)$$

To form the global transfer matrix of the whole symmetrical porous aggregate with dead-end porosity, the chain rule on transfer matrix multiplication is used. This gives

$$\begin{Bmatrix} P \\ U \end{Bmatrix} = [T]^S \begin{Bmatrix} P'' \\ -U'' \end{Bmatrix}, \qquad (40)$$

with

$$[T]^S = [T]_A [T]_B . \qquad (41)$$

Remarks :

a) This transfer matrix has the following properties: reciprocity (i.e., $\det[T]^S = 1$), symmetry of the material (i.e., $t_{11}^s = t_{22}^s$), and compatibility with other classical transfer matrices.[2]

b) This approach can be adapted to heterogeneous dead-end materials with different dead-end parameters on each half.

c) If $[T]_A$ is computed with thickness *l* instead of *l*/2, then the non-symmetric matrix $[T]^{NS}$ of paragraph F.1 is found. If $[T]_B$ is computed with thickness *l* instead of *l*/2, then a similar non-symmetric model is found; however this time the dead-end pores are localized on the

other side. In conclusion, the symmetric transfer matrix model encompasses the non-symmetric model and is therefore more general.

G. Acoustical indicators

G-1 Sound transmission loss

From the transfer matrix approach, it is easy to study the sound transmission of a porous material with dead-end porosity. The global transfer matrix of a porous media with dead-end porosity is $[T]^{mat}$. This matrix must be adapted to the particular case under study. If a non-symmetric configuration with dead-end pores on the front face is considered, then $[T]^{mat} = [T]^{NS} = [T(l)]_A$. If the dead-end pores are on the rear face, then $[T]^{mat} = [T(l)]_B$. If a symmetric configuration is considered, then $[T]^{mat} = [T]^{S}$. From the appropriate transfer matrix, the sound transmission coefficient and the transmission loss in normal incidence are given by:

$$|\tau| = \left| \frac{2}{t_{11}^{mat} + t_{22}^{mat} + t_{12}^{mat}/Z_0 + t_{21}^{mat} Z_0} \right|, \qquad (42)$$

and

$$TL = -20\log_{10}(|\tau|), \qquad (43)$$

where Z_0 is the characteristic impedance of the air.

G-2 Sound absorption coefficient

To obtain the sound absorption coefficient from the transfer matrix method, one needs first to define the backing condition and use the appropriate system transfer matrix $[T]^{syst}$. If the porous material with dead-end porosity is backed by a rigid wall $[T]^{syst} = [T]^{mat}$. If the porous material with dead-end porosity is backed by an air cavity and a rigid wall, $[T]^{syst} = [T]^{mat}[T]^{cav}$ with

$$[T]^{cav} = \begin{bmatrix} \cos(k_0 l_{cav}) & jZ_0 \sin(k_0 l_{cav}) \\ \frac{j}{Z_0}\sin(k_0 l_{cav}) & \cos(k_0 l_{cav}) \end{bmatrix}, \qquad (44)$$

where k_0 is the wave number of air, and l_{cav} is the depth of the cavity. Then, from the appropriate system transfer matrix, the normal incidence surface impedance of the studied configuration is given by:

$$Z_S = \frac{t_{11}^{syst}}{t_{12}^{syst}}. \qquad (45)$$

and the normal sound absorption coefficient by:

$$\alpha_N = 1 - \left| \frac{Z_S - Z_0}{Z_S + Z_0} \right|^2. \qquad (46)$$

III. EXPERIMENTAL RESULTS

A. Simplified sample

To confirm the validity of the exposed model, a simplified non-symmetric sample with well-controlled parameters was tested. The sample consists of a circular column of Teflon which is perforated with regular cylindrical perforations (see Figure 10). Some perforations are complete (they represent the kinematic porosity), others are incomplete or semi-closed (they represent the dead-end porosity). The open ends are only visible on one face of the sample (Face A). The depth of the semi-closed holes is l_{DE} = 25 mm, the sample thickness is l = 30 mm, its diameter is 44.4 mm, the perforation diameter is d = 2 mm, and the minimum perforation constriction is d_{min} = 1.8 mm (error due to the perforation process). The porosities are ϕ_B = 14 %, ϕ_{DE} = 13.5 %. Table 1 summarizes the dead-end parameters of the tested sample.

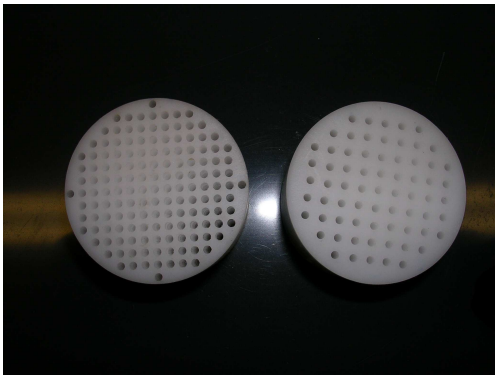

Figure 10: Photo of simplified non-symmetric sample. Face A (left) includes all pores. Face B (right) only includes effective pores (without dead-end pores).

Total porosity (%)	ϕ_B (%)	ϕ_{DE} (%)	l_{DE} (mm)
27.5	14	13.5	25

Table 1: Dead-end parameters of the non-symmetric simplified sample.

For this kind of simple material, the Johnson-Champoux-Allard's (JCA) parameters are easily defined for both the Biot and DE domains. The viscous and thermal lengths, the tortuosity and the resistivity are given respectively by JCA's parameters for cylindrical pores:[2] $\Lambda' = d / 2$, $\Lambda = d_{min} / 2$, $\alpha_\infty = 1$, and $\sigma = 32\eta/\phi d^2$, where η is the dynamic viscosity of air and ϕ is the open porosity (use ϕ_B for the Biot domain; use ϕ_{DE} for the DE domain). Since the sample thickness is large compared to the perforation diameter, the sound radiation of the perforation openings in open air is not considered here.

A three-microphone impedance tube is used to measure the normal sound absorption coefficient and sound transmission loss of the sample coupled to an air cavity and a rigid termination. The frequency range was chosen between 200 Hz and 4200 Hz to make sure that only plane waves exist in the tube (the tube diameter is 44.45 mm, the cut-off frequency is 4400 Hz). The two microphones upstream the sample are used to measure the sound absorption by the standard impedance tube measurement technique[20]. Since the simplified sample is non-symmetric, the sound absorption coefficient of each face will be measured. A third microphone, localized on the hard wall backing (behind the backing cavity), measures the transfer matrix and deduces the transmission loss by way of the "three-microphones and two-cavity method" [21]. For the transmission loss measurement, the choice of surface exposition of the non-symmetrical material is not important since reciprocity principle applies on transmission. The sound pressure excitation is random noise in linear regime. The majority of repeatability errors come from the way the sample is positioned in the tube: special attention was therefore paid to this positioning. However, as this error is low for these measurements, their associated error bars are not presented graphs.

The results which are presented on Figures 11 and 12 correspond to the configuration where face A (showing the dead-end pores) is on the source side. Figure 11(a) shows the comparison between experimental results and models' predictions (present model and JCA model) of the absorption coefficient of the simplified non-symmetric sample coupled to a 20-mm air cavity gap and a rigid wall. The present model with the non-symmetric transfer matrix given by $[T(l)]_A$ is used. The first absorption peak (around 750 Hz) represents the air cavity effect, and the second peak (around 3300 Hz) represents the semi-closed hole effect (i.e., dead-end porosity effect) on the excitation side. Compared to the JCA model (where only kinematic porosity is taken into account), the present model improves the comparison with experiments. In fact, the present model precisely predicts the frequency position of the two peaks, although the absorption peak values are slightly different. The comparison between experiments and predictions for a different air cavity gap (l_{cav} = 50 mm) is presented in Figure 11(b). Around 3300 Hz, the air cavity effect and the dead-end porosity effect are coupled on the absorption coefficient: note that the present model accounts for this coupling effect.

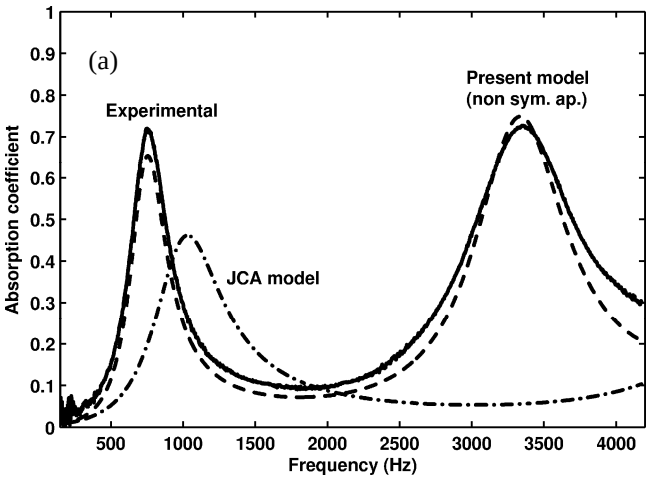

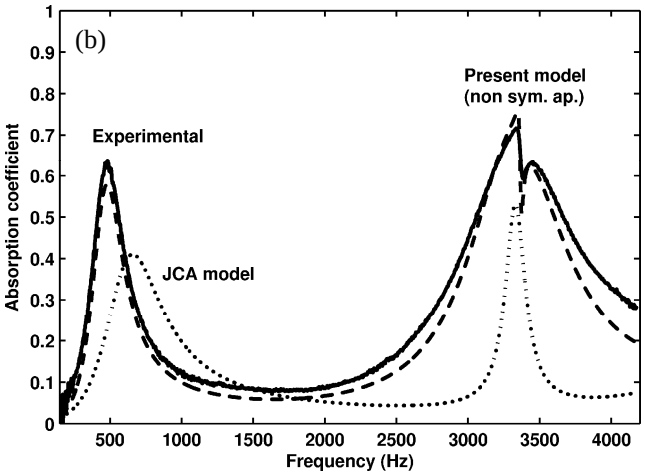

Figure 11: Comparison between experimental results and models' predictions of the absorption coefficient of the simplified non-symmetric sample coupled to an air cavity and a rigid wall. Face A (showing dead-end pores) is on the source side. (a) 20-mm thick air cavity. (b) 50-mm thick air cavity.

Figure 12 presents the comparison between experimental results and models' predictions of the transmission loss of the simplified non-symmetric sample. Here, the presence of the dead-end pores significantly modifies the transmission loss: a large peak of transmission loss appears around 3300 Hz. The frequency position of this transmission loss peak is quite dependent on the value of l_{DE}. Good agreement is obtained between the present model and the experimental results.

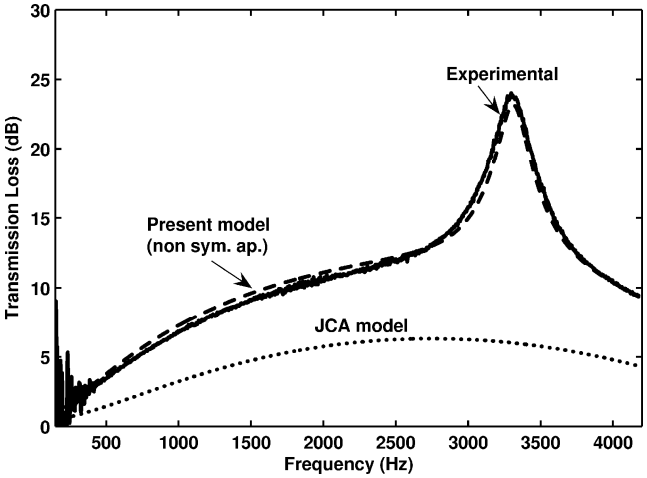

Figure 12: Comparison between experimental results and models' predictions of the transmission loss of the simplified non-symmetric sample. Face A (showing dead-end pores) is on the source side.

Figures 13 and 14 present the sound absorption and transmission loss of the same simplified non-symmetric sample but this time the sample is inverted in the tube. Contrary to the previous results, the dead-end pores (face A) are now facing the backing air cavity and rigid wall. Hence, the non-symmetric matrix given by $[T(l)]_B$ is used. Figure 13 presents the comparison between experiments and predictions for the absorption coefficient of the simplified non-symmetric sample coupled to two different air cavity gaps: l_{cav} = 20 mm and l_{cav} = 50 mm. The experimental and simulated results are logically quite different compare to the preceding part particularly concerning the absorption peak caused by the DE pores. For l_{cav} = 20 mm, this peak almost disappears. Only a very small peak emerges around 3300 Hz. For l_{cav} = 50 mm, three absorption peaks can be observed: the two first correspond to the Biot pore coupled with air cavity effect, while the third peak corresponds to the DE pore coupled with air cavity effect. For the sound absorption coefficient, the comparison between the experimental results and the present model's predictions is satisfactory.

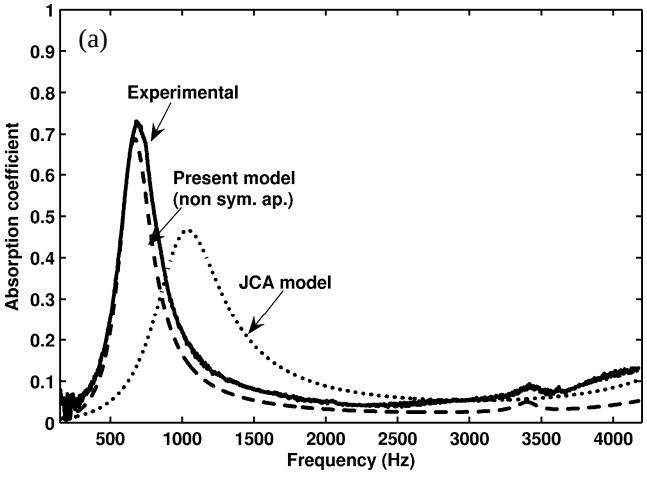

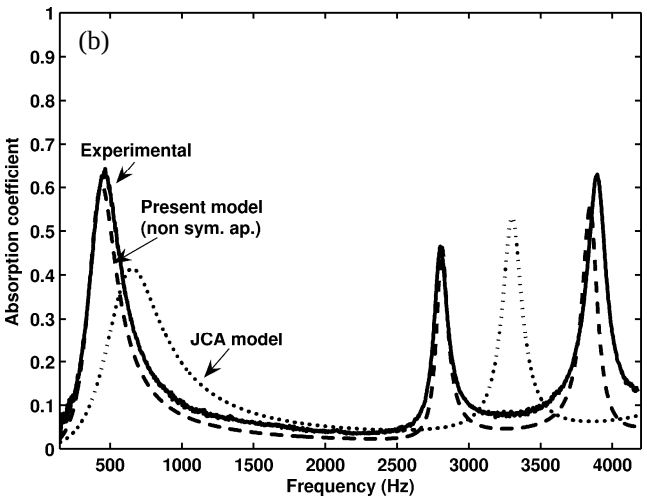

Figure 13: Comparison between experimental results and models' predictions of the absorption coefficient of the simplified non-symmetric sample coupled to an air cavity and a rigid wall. Face A (showing dead-end pores) is on the backing cavity side. (a) 20-mm thick air cavity. (b) 50-mm thick air cavity.

In Figure 14, the simulated transmission loss in the inverted configuration is logically equivalent to the one previously obtained in Figure 12 due to the reciprocity of the transfer matrix. Similarly, the experimental results are not very different from those presented in Figure 12. The slight differences may be attributed to experimental errors and to the positioning in the tube when the sample was inverted.

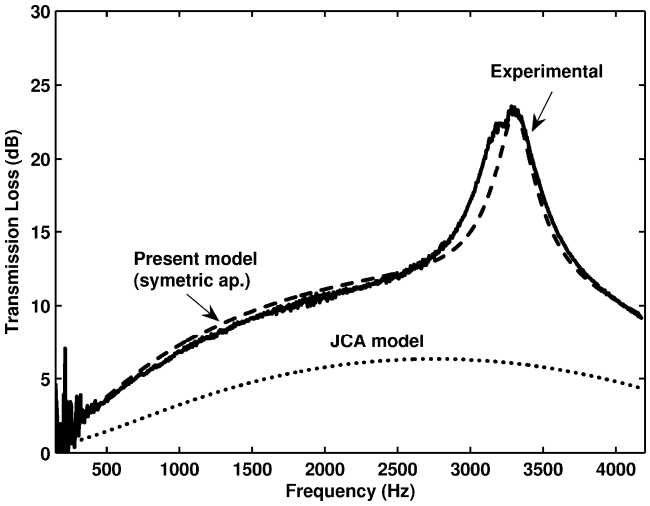

Figure 14: Comparison between experimental results and models' predictions of the transmission loss of the simplified non-symmetric sample. Face A (showing dead-end pores) is on the source side.

In this section a simplified sample was presented to validate the present model and to show the importance of accounting for dead-end porosity. The comparisons between the predictions of the present model and the experimental results are in good agreement for both the sound absorption coefficient and the sound transmission loss. Similar results were also obtained for a series of other simplified non-symetrical samples with different parameters. For the sake of simplicity, these results were not reported here. The following section will test the present model with a more complex and more realistic material than the simplified non-symmetrical sample.

B. Aluminum foam sample

In this study, a number of different aluminum foams were tested and one has been selected for presentation in this article (see Figure 15). The base material used was AS7G Aluminum. The Johnson-Champoux-Allard's (JCA) parameters of the aluminum foam have been first measured. The static airflow resistivity σ and global porosity ϕ have been respectively measured by a resistivity-meter and a weight differential approach.[22,23] To characterize the tortuosity α_∞ and characteristic lengths Λ and Λ', the ultrasound method have been used[24-27]. This method allows measuring the equivalent length

$$L_{eq} = \left(\frac{1}{\Lambda} + \frac{\gamma - 1}{B\Lambda'} \right)^{-1}, \qquad (47)$$

where γ is the adiabatic constant of gas and B^2 is the Prandtl number.

The L_{eq} values were found to be very weak, suggesting that constrictions between two cells are very narrow. This can be seen on the microstructure pictures (Figure 2), which also allows observing the pore size. The ratio between Λ' and Λ was difficult to find; the typical ratio for classical material is generally between 2 and 4. Therefore, image analysis was used to estimate Λ'/Λ: microscope pictures of transversal and longitudinal cross-sections of a material sample were taken with different light incidences. Following this procedure, the mean pore size of the foam (d_{cell}) and the size of interstices (d_{hole}) were obtained. In a first approximation, the ratio Λ'/Λ was identified by the ratio d_{cell} / d_{hole}.

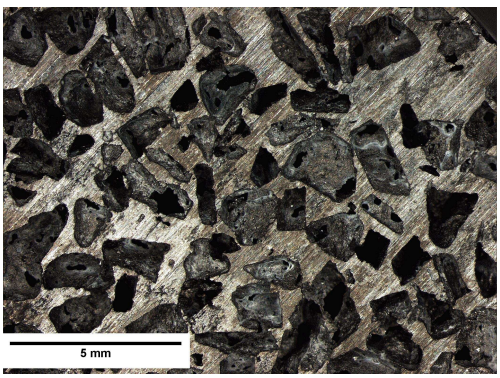

Figure 15: Photo of the surface of the tested aluminum foam.

These experimental methods to define the JCA parameters introduce significant errors when applied to metallic foams; therefore, it is important to define for each JCA parameter a mean value $\bar{x}$ and a standard deviation $\sigma_{st.dev.}$, such that $x = \bar{x} \pm \sigma_{st.dev.}$. These errors were then included in the models (JCA and present models). On the figures, the models' predictions are represented with their error bars. The JCA acoustic parameters (mean value and standard deviation) are summarized in Table 2. As it will be shown, the errors on the JCA parameters introduce notable errors on the predictions of the transmission loss and sound absorption coefficient, which are more significant than those obtained with impedance tube measurements. To facilitate readability of the results, only the error bars on the predictions are presented in the figures.

JCA parameters	Λ (μm)	Λ' (μm)	α_∞	σ (Pa.s/ m²)	ϕ (%)
Mean value	101	352	2.25	19713	64.5
Standard deviation	4	14	0.05	300	3

Table 2: Johnson-Champoux-Allard (JCA) parameters of the aluminum foam sample.

To take into account the dead-end porosity effect, the dead-end parameters (l_{DE} and ϕ_{DE}) had to be determined. For l_{DE}, a multiple of the statistical pore size was chosen: $l_{DE} = n\, d_{cell}$. To determine n and ϕ_{DE}, a fitting approach on the experimental results was used. As it is very difficult to define precisely l_{DE} and ϕ_{DE} for these kinds of complex foams, works are in progress to estimate them notably from micro-tomography and ultrasound methods. The used dead-end parameters (mean value and standard deviation) are summarized in Table 3.

Total porosity (%)	ϕ_B (%)	ϕ_{DE} (%)	l_{DE} (mm)
64.5 ± 3	≈ 55	≈ 7.5	≈ $7d_{cell}$

Table 3: Dead-end parameters of the aluminum foam sample (fitting and experimental approaches).

For this kind of material, it is preferable to use the symmetric transfer matrix $[T]^S$ for predicting its acoustical indicators. In fact, due to the random nature of the fabrication process, the dead-end pores are dispersed throughout the material in a homogeneous manner.

Remark :

At this stage of the research, we have chosen to use the same JCA parameters, measured on the global aluminium foams (see preceding part), for both the DE element (Λ_{DE}, Λ'_{DE}, $\alpha_{\infty DE}$, σ_{DE}) and Biot kinematic element (Λ_B, Λ_B, $\alpha_{\infty B}$, σ_B). The choice of these parameters will have to be studied more precisely in the future.

As in the previous section, the impedance tube with two-microphone technique is used to measure the sound absorption and the three-microphone technique is used to measure the sound transmission loss.

Figure 16 presents the comparison between experimental results and models' predictions ($[T]^S$ symmetric approach and JCA model) of the absorption coefficient of the studied aluminum foam sample coupled to: (a) a rigid wall (l_{cav} = 1 mm), and (b) a 50-mm air cavity backed by a rigid wall. One can note that the present approach and JCA model yield comparable results in terms of sound absorption and compare well with experimentations. However, a slight shift towards low frequencies is observed with the present symmetric approach. This yields a better prediction of the absorption peaks. This seems to show that the present approach adds the necessary degree-of-freedom to capture the physics of the dead-end pores in the material, which are not captured with the JCA model.

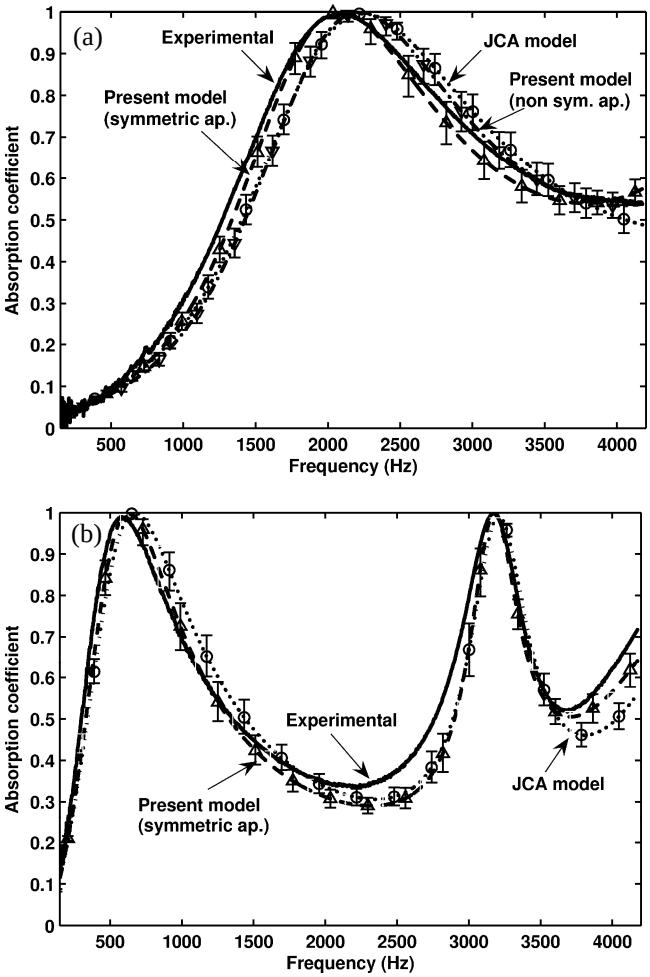

Figure 16: Comparison between experimental results and models' predictions of the absorption coefficient of the aluminum foam sample. (a) Hard wall backing (l_{cav} < 1 mm). (b) Air cavity backing (l_{cav} = 50 mm) on hard wall.

Figure 17 presents the comparison between experimental results and models' predictions of the transmission loss of the aluminum foam sample. The comparison between the present model and the experiment results is encouraging. Here, it is clear that the JCA model does not capture the effects of dead-end pores, even considering error bars on the prediction; by contrast, the present model with its error bars always includes the experimental curve for the entire frequency band.

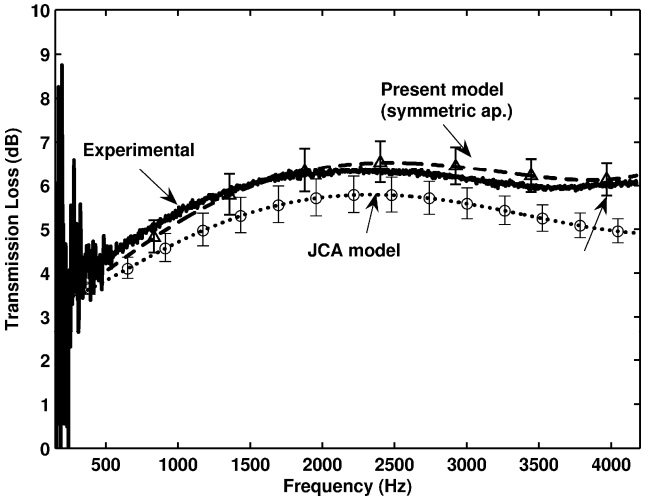

Figure 17: Comparison between experimental results and models' predictions of the transmission loss of the aluminum foam sample.

Generally, the present model improves the comparison with experimental results for a part of all the tested aluminum foams. However, for certain foam samples, the proportion of dead-end porosity is weak and the dead-end effect on the sound absorption and sound transmission loss is low (i.e., modifications are of the order of the estimation errors of the dead-end parameters). Moreover, more research and experiments on a greater number of samples are necessary in order to improve the experimental methods and to define more precisely the two dead-end parameters.

IV. CONCLUSIONS

In this study, the acoustic properties of materials with dead-end porosity were examined, and in particular a certain class of metallic foams. For these materials, the classical fluid model predictions such as Johnson-Champoux-Allard model are not as satisfying as for other materials.

From a microscopic analysis of dead end pores, a simple model that offers a correction taking into account this complex micro-geometry was proposed. After a homogenization process, two acoustic transfer matrix approaches were investigated: one for non symmetric dead-end element, and the second for symmetric dead-end element. It appears that the

symmetric matrices modeling encompasses the non symmetric modeling and is therefore more general.

To validate this model, materials with well controlled parameter and including dead-end pores ("simplified samples") were tested. With the use of an impedance tube and the two- and three-microphone technique, the coefficients of absorption and transmission loss were measured. It was found that the comparison between the present model and the experimental results is much more flattering and the importance of accounting for dead-end porosity is noticed. Measurements on metallic foams show that an improvement on theoretical predictions can be obtained with this correction. However for certain metallic foams, the influence of dead-end porosity introduces modifications of the order of estimation errors on these parameters and thus do not allow for definite conclusions.

It is utmost importance to develop new theoretical and experimental research on the two new parameters l_{DE} and ϕ_{DE} (for example: micro-tomography, ultrasonic characterization, comparison of different ϕ measurements, theoretical study of these materials in bottom-up approaches). It is also necessary to refine the methods of evaluation of JCA parameters (notably α_∞, Λ, Λ') and to reduce the uncertainty of the measurements.

[1] X. L. Gong, Y. Liu, SY. He & J. Lu, “Manufacturing and low-velocity impact response of a new composite material, Metal Porous Polymer Composite”, Journal of Materials Science and Technology 20, 65-68 (2004).
[2] J. F. Allard and N. Atalla, *Propagation of Sound in Porous Media : Modelling Sound Absorbing Materials*, Wiley and Sons Ltd, 2009.
[3] J. F. Allard, P. Herzog, D. Lafarge and M. Tamura, “Recent topics concerning the acoustics of fibrous and porous materials”, Applied Acoustics 39(1-2), 3-21 (1993).
[4] Y. Champoux and J.F. Allard, “Dynamic tortuosity and bulk modulus in air-saturated porous media,” J. Appl. Phys. 70, 1975-1979 (1991).
[5] T. Bourbié, O. Coussy and B. Zinsner , Acoustique des milieux poreux, Technip (1986).
[6] C. Zwikker and C. W. Kosten, *Sound absorbing materials*, Elsevier, New York, 174 p., 1949.
[7] J. Bear, *Hydraulics of Groundwater*. McGraw-Hill, New York, 576 p., 1979.
[8] P. Gibb, M. J. Barcelona, J. D. Ritchey, M. H. LeFaivre, “Effective porosity of geologic material – First annual report”. Report for State Water Suvey Division – ENR – Illinois department, September 1984.
[9] P. Habisreuther, N. Djordjevic and N. Zarzalis, “Statistical distribution of residence time and tortuosity of flow through open-cell foams”. Chemical Engineering Science 64, 4943-4954 (2009).
[10] I. Fatt, “Influence of dead end pores on relative permeability of porous media”. Science 134, 1750 – 1751 (1961).
[11] E. A. Moreira, M. D. M. Innocentinib and J. R. Courya, “Permeability of ceramic foams to compressible and incompressible flow”, Journal of the European Ceramic Society 24, 3209–3218 (2004).
[12] F. Chevillotte, C. Perrot, and R. Panneton. “Microstructure based model for sound absorption predictions of perforated closed-cell metallic foams,” J. Acoust. Soc. Am. 128 (4), 1766-1776 (2010).
[13] P. Leclaire, T. Dupont, O. Sicot, and X. L. Gong, Propriétés acoustiques de matériaux poreux saturés d'air incluant une porosité partiellement ouverte, Proceeding CFA, Lyon avril 2010.
[14] K. V. Horoshenkov and M. J. Swift, “The acoustic properties of granular materials with pore size distribution close to log-normal”, J. Acoust. Soc. Am. 110, 2371-2378 (2001).
[15] D. T. Blackstock, Fundamentals of physical acoustics, Wiley and Sons Inc., 2000.
[16] M. A. Biot, “Theory of propagation of elastic waves in a fluid saturated porous solid. I. Low-frequency range”, J. Acoust. Soc. Am. 28, 168-178 (1956).
[17] M. A Biot, “Theory of propagation of elastic waves in a fluid saturated porous solid. II. Higher frequency range”, J. Acoust. Soc. Am. 28, 179-191 (1956).
[18] D. L. Johnson, J. Koplik and R. Dashen, “Theory of dynamic permeability and tortuosity in fluid saturated porous media”, J. Fluid. Mech. 176, 379-402 (1987).
[19] R. Panneton, “Comments on the limp frame equivalent fluid model for porous media”, J. Acoust. Soc. Am 122 (6), EL217-EL222 (2007).
[20] ISO-10534-2, “Acoustics—Determination of sound absorption coefficient and impedance in impedance tubes. Part 2: Transfer-function method,” International Organization for Standardization, Geneva, Switzerland 1998.
[21] Y. Salissou, R. Panneton, and O. Doutres, “Three-microphone method for measuring the normal sound transmission loss of noise control samples in standing wave tube,” submitted for publication in Applied Acoustics (2010).
[22] M.R. Stinson et G.A Daigle, “Electronic system for the measurements of flow resistance,” J. Acoust. Soc. Am. 83, 2422-2428 (1988).
[23] Y. Salissou and R. Panneton, “Pressure/ Mass method to measure open porosity,” J. App. Phys. 101, 124913.1-124913.7 (2007).

[24] P. Leclaire, L. Kelders, W. Lauriks, C. Glorieux and J. Thoen, “Determination of the viscous characteristic length in air-filled porous materials by ultrasonic attenuation measurements”, J. Acoust. Soc. Am. 99, 1944-1948 (1996).

[25] B. Brouard, B. Castagnède, M. Henry, D. Lafarge and S. Sahraoui, “Mesure des propriétés acoustiques des matériaux poreux”, Techniques de l’ingénieur, R 6 120 (2003).

[26] Z. E. A. Fellah, S. Berger, W. Lauriks, C. Depollier, C. Aristegui and J.-Y. Chapelon, “Measuring the porosity and the tortuosity of porous materials via reflected waves”, J. Acoust. Soc. Am. 113 (5), 2424-2433 (2003).

[27] F. Fohr, D. Parmentier, B. Castagnède and M. Henry, “An alternative and industrial method using low frequency ultrasound enabling to measure quickly tortuosity and viscous characteristic length”, Proceeding Acoustics‘08, Paris, 30 June – 4 July (2008).

Figure 14: Comparison between experimental results and models' predictions of the transmission loss of the simplified non-symmetric sample. Face A (showing dead-end pores) is on the source side.

Figure 15: Photo of the surface of the tested aluminum foam.

Figure 16: Comparison between experimental results and models' predictions of the absorption coefficient of the aluminum foam sample. (a) Hard wall backing (l_{cav} < 1 mm). (b) Air cavity backing (l_{cav} = 50 mm) on hard wall.

Figure 17: Comparison between experimental results and models' predictions of the transmission loss of the aluminum foam sample.